FULL PAPER

Conjugated Polymer Amplified Far-Red/Near-Infrared Fluorescence from Nanoparticles with Aggregation-Induced Emission Characteristics for Targeted In Vivo Imaging

Dan Ding, Kai Li, Wei Qin, Ruoyu Zhan, Yong Hu, Jianzhao Liu, Ben Zhong Tang, and Bin Liu*

Fluorescence-amplified far-red/near-infrared (FR/NIR) nanoparticles (NPs) are synthesized by co-encapsulation of conjugated polymer donor (poly[9,9-bis(2-(2-(2-methoxyethoxy)ethoxy)ethyl)fluorenyldivinylene]; PFV) and a fluorogen acceptor (2-(2,6-bis((E)-4-(phenyl(4′-(1,2,2-triphenylvinyl)-[1,1′-biphenyl]-4-yl)amino)styryl)-4H-pyran-4-ylidene)malononitrile; TPE-TPA-DCM) with aggregation-induced emission (AIE) characteristics using biocompatible bovine serum albumin (BSA) as the encapsulation matrix. The good spectral overlap and close proximity between PFV and TPE-TPA-DCM in BSA NPs result in a 5.3-fold amplified TPE-TPA-DCM emission signal via fluorescence resonance energy transfer (FRET). The obtained PFV/TPE-TPA-DCM co-loaded BSA NPs are spherical in shape with a large Stokes shift of ∼223 nm and low cytotoxicity. The BSA matrix allows further functionalization with arginine-glycine-aspartic acid (RGD) peptide to yield fluorescent probes for specific recognition of integrin receptor-overexpressed cancer cells. The advantage of PFV amplified FR/NIR signal from TPE-TPA-DCM is further demonstrated in cellular and in vivo imaging using HT-29 colon cancer cells and a murine hepatoma H_{22} tumor-bearing mouse model, respectively. The high FR/NIR fluorescence and specific cancer targeting ability by RGD surface functionalization make the PFV/TPE-TPA-DCM co-loaded BSA-RGD NPs a unique FR/NIR fluorescent probe for cellular imaging and in vivo tumor diagnosis in a high contrast and selective manner.

1. Introduction

Development of efficient fluorescent probes with intense far-red/near-infrared (FR/NIR) emission (>650 nm) and large Stokes shifts is of great importance in cancer research.[1] The fluorescence in FR/NIR region is a unique interrogation window for cellular and in vivo bioimaging with low interferential absorption and limited biological autofluorescence.[2] The large Stokes shift can minimize the interference between excitation and emission, as well as shift the emission spectrum away from the sample autofluorescence to result in high detection sensitivity.[3] So far, organic fluorophores[4] and inorganic semiconductor quantum dots (QDs)[5] have been widely used as FR/NIR fluorescent probes for in vitro and in vivo cancer diagnosis. Organic FR/NIR fluorophores often have poor photostability and small Stokes shifts.[6] In addition, water-dispersible FR/NIR emitters generally have planar aromatic structures which make them vulnerable to aggregate via π–π stacking or upon interaction with bioanalytes. This can lead

Dr. D. Ding, R. Y. Zhan, Prof. B. Liu
Department of Chemical and Biomolecular Engineering
National University of Singapore, 117576, Singapore
E-mail: cheliub@nus.edu.sg

W. Qin, Dr. J. Liu, Prof. B. Z. Tang
Department of Chemistry
Institute for Advanced Study
State Key Laboratory of Molecular Neuroscience
Institute of Molecular Functional Materials
and Division of Biomedical Engineering
The Hong Kong University of Science and Technology (HKUST)
Clear Water Bay, Kowloon, Hong Kong, China

Prof. Y. Hu
National Laboratory of Solid-State Microstructure
Department of Material Science and Engineering
Nanjing University, Nanjing 210093, China

Dr. K. Li, Prof. B. Z. Tang, Prof. B. Liu
Institute of Materials Research Engineering
3 Research Link, 117602, Singapore

Prof. B. Z. Tang
South China University of Technology
(SCUT)-HKUST Joint Research Laboratory
Guangdong Innovative Research Team
State Key Laboratory of Luminescent Materials and Devices
South China University of Technology
Guangzhou 510640, China

DOI: 10.1002/adhm.201200243

www.MaterialsViews.com

**ADVANCED
HEALTHCARE
MATERIALS**
www.advhealthmat.de

FULL PAPER

to non-radiative processes, which will significantly reduce their fluorescence, known as aggregation-caused quenching (ACQ).[7] As compared to organic fluorophores, QDs could provide higher fluorescence, improved photostability and larger Stokes shifts.[8] However, the oxidative degradation of the heavy metal components of QDs leads to the release of heavy metal ions, which are highly toxic to biological species.[9] The increasing interest in bioimaging and cancer diagnosis motivates us to pursue alternative FR/NIR fluorescent probes that can overcome the limitations of poor photostability, small Stokes shift, ACQ effect and high toxicity.

Recently, we have developed a new category of organic luminogens, which have the opposite characteristics to ACQ effect. These luminogens show unique aggregation-induced emission (AIE) feature.[10] AIE luminogens are often propeller-shaped. The dynamic rotations of their aromatic rotors non-radiatively deactivate their excited states in the solution state to yield weak fluorescence. In the aggregate state, the propeller shape of the molecules prevents π–π stacking and blocks the ACQ pathway. The restriction of the intramolecular rotations (RIR) opens radiative decay channel and the luminogens are highly fluorescent when aggregated.[10] AIE luminogens can be chemically modified to be water-soluble, which require multiple synthetic steps and long reaction time. As compared to the sophisticated modification of AIE luminogen structures, two strategies have been developed to directly transform organic soluble AIE luminogens into aqueous media for bioimaging applications. One is to form nanoaggregates by direct addition of water to a stock solution of AIE luminogens in water-miscible organic solvents, such as THF and DMSO.[11] The other is to encapsulate AIE luminogens using block copolymers or biocompatible proteins as the matrix to form nanoparticles (NPs).[3,12] Although these nanomaterials show good photostability and low cytotoxicity in cellular imaging, very few have shown FR/NIR emission and their applications in targeted in vivo imaging remain unexplored. Additionally, probes with high brightness are always desirable to achieve good imaging contrast at minimum dosage.[13]

As compared to sophisticated chemical modifications to improve the brightness of each fluorophore, fluorescence resonance energy transfer (FRET) is a powerful spectroscopic tool to enhance fluorescence signals and increase apparent Stokes shift of fluorescent probes for biological sensing and imaging.[14] It takes advantage of the light-harvesting property of the donor to enhance the acceptor fluorescence when they are within close proximity.[15] In this regard, conjugated polymers (CPs) are effective light-harvesting energy donors due to their π-conjugated backbones and large absorption coefficients,[16] which have been reported to enhance the fluorescence of various fluorescent materials, such as organic fluorophores,[17] fluorescent proteins,[18] QDs[19] and gold nanoclusters.[20] In addition, recent studies have revealed that CP-based nanoprobes show high brightness, good photostability and low cytotoxicity, which make them ideal candidates for in vitro and in vivo imaging applications.[2c,13,21] By virtue of these desirable features, a CP is selected in this study to pair with an FR/NIR AIE luminogen to constitute the first signal amplified FR/NIR probe for live-animal imaging and cancer diagnosis.
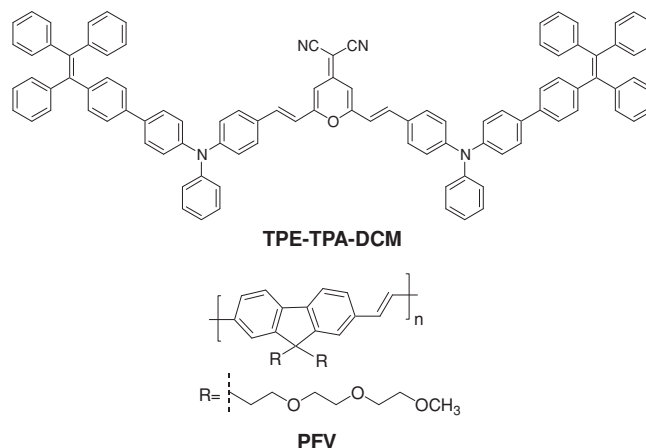
Scheme 1. Chemical structures of TPE-TPA-DCM and PFV.

To demonstrate the concept, in this contribution, poly[9,9-bis(2-(2-(2-methoxyethoxy)ethoxy)ethyl)fluorenyldivinylene] (PFV,[21b] **Scheme 1**), a green-emitting CP, was used as a FRET donor, while 2-(2,6-bis((E)-4-(phenyl(4′-(1,2,2-triphenylvinyl)-[1,1′-biphenyl]-4-yl)amino)styryl)-4H-pyran-4-ylidene)malononitrile (TPE-TPA-DCM,[12] Scheme 1), an FR/NIR AIE-emitter, was selected as an acceptor. The donor-acceptor pair was co-encapsulated into biocompatible bovine serum albumin (BSA) NPs at different donor-acceptor ratios to maximize the acceptor emission. Spectroscopy studies reveal that under optimized conditions, the polymer amplified TPE-TPA-DCM emission is over 5-fold brighter as compared to that from the same amount of acceptor upon direct excitation. Subsequent functionalization of the BSA NPs with arginine-glycine-aspartic acid (RGD) peptide led to surface functionalized NPs, which have been successfully used for targeted cancer cell imaging and in vivo imaging in a high contrast and specific manner.

As FRET requires the donor and acceptor chromophores to be located within close proximity, AIE luminogens are ideal fluorescent acceptors as they show bright fluorescence in the aggregated states. So far, successful examples of fluorescence amplified AIE probes for bioimaging applications have been rarely exploited and there is no demonstration of their application in targeted in vivo imaging.[3] This study thus opens up new opportunities for the development of a new generation of promising probes for the advancement of bioimaging.
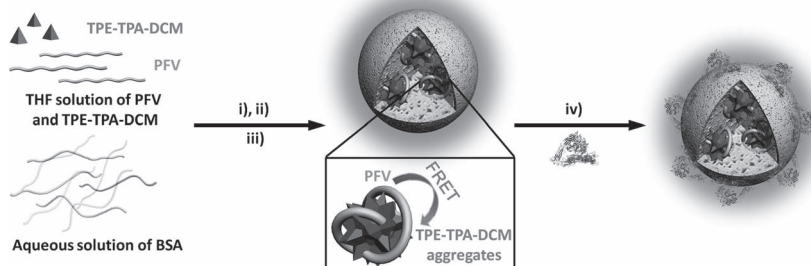
2. Results and Discussion

2.1. Synthesis and Characterization of PFV/TPE-TPA-DCM co-Loaded BSA NPs

Scheme 1 shows the chemical structures of TPE-TPA-DCM and PFV. TPE-TPA-DCM was synthesized by conjugating a paradigm of AIE luminogens, tetraphenylethene (TPE), to 2-(2,6-bis((E)-4-(diphenylamino)styryl)-4H-pyran-4-ylidene)malononitrile (TPA-DCM).[12] The TPE-TPA-DCM could form nanoaggregates upon

ADVANCED
HEALTHCARE
MATERIALS
www.advhealthmat.de

Materials
Views
www.MaterialsViews.com

FULL PAPER

gradual addition of water into the luminogen solution in tetrahydrofuran (THF) and the fluorescence intensity of TPE-TPA-DCM is significantly increased with increasing the water fractions (f_w) in THF/water mixtures from 50% to 90%, demonstrating the unique AIE feature of TPE-TPA-DCM (Figure S1 in the Supporting Information (SI)). **Figure 1** shows the absorption and photoluminescence (PL) spectra of PFV and TPE-TPA-DCM in THF. PFV has two absorption maxima at 425 and 455 nm. The emission spectrum of PFV has a maximum at 467 nm and a shoulder at 498 nm. On the other hand, TPE-TPA-DCM shows two absorption bands centered

Scheme 2. Schematic illustration of the synthesis of PFV/TPE-TPA-DCM co-loaded BSA NPs and PFV/TPE-TPA-DCM co-loaded BSA-RGD NPs. (i) sonication; (ii) cross-linking; (iii) THF removal; (iv) RGD peptide functionalization.

at 350 and 486 nm with an emission maximum at 633 nm. Noteworthy is that the emission spectrum of PFV overlaps well with the absorption spectrum of TPE-TPA-DCM, indicating that they may form a good donor-acceptor pair for FRET. It is expected that FRET could occur when PFV and TPE-TPA-DCM are brought into close proximity when they are co-encapsulated into NPs.

Bovine serum albumin (BSA) was selected as the polymer matrix for NP formulation due to its biocompatibility and non-toxicity.[22] The PFV/TPE-TPA-DCM co-loaded BSA NPs were synthesized through a modified desolvation method.[23] As shown in **Scheme 2**, the NP synthesis started with the addition of a THF solution containing TPE-TPA-DCM and PFV into BSA aqueous solution under sonication, which was followed by cross-linking with glutaraldehyde and THF removal. During NP formation, the TPE-TPA-DCM aggregates tend to be entangled with PFV and the hydrophobic domains of BSA to afford the hydrophobic interiors of the NPs. The negative zeta potentials of the obtained NPs in aqueous solution (~−30 mV) indicate that the outermost layer of the PFV/TPE-TPA-DCM co-loaded BSA NPs contains ionized carboxylic groups, which stabilize the NPs through electrostatic repulsion. The similar strategy has also been used to synthesize BSA NPs containing

TPE-TPA-DCM or PFV only. As compared to copolymerization of donor and acceptor monomers or covalent conjugation of donor and acceptor molecules to achieve FRET, this strategy of donor/acceptor co-encapsulated into one NP is simple to operate, which minimizes the tedious synthetic efforts.

To optimize the FR/NIR emission, PFV/TPE-TPA-DCM co-loaded BSA NPs with various donor/acceptor molar ratios were synthesized and characterized. Table S1 in the SI summarizes the encapsulation efficiencies (EEs) and average sizes of the PFV/TPE-TPA-DCM co-loaded BSA NPs synthesized at various feeding concentrations of PFV. The feeding concentrations of TPE-TPA-DCM and BSA are fixed at 0.01 and 1.5 mg/mL, respectively. As shown in Table S1, although the EEs of both PFV and TPE-TPA-DCM decrease with the increased PFV feed, all the NPs have a relatively high EE (>70%) for PFV and TPE-TPA-DCM. According to the EEs, the molar ratios of PFV based on repeat unit (RU) to TPE-TPA-DCM based on molecule loaded in BSA NPs ([PFV RU]/[TPE-TPA-DCM]) are determined to be 0:1, 4.9:1, 9.6:1, 14.2:1 and 18.8:1, respectively, at different feeding concentrations of PFV. In addition, laser light scattering (LLS) results suggest that the average sizes of the PFV/TPE-TPA-DCM co-loaded BSA NPs increase from 125 to 159 nm with the increase of [PFV RU]/[TPE-TPA-DCM] from 0:1 to 18.8:1. The larger average size of PFV/TPE-TPA-DCM co-loaded NPs than that of TPE-TPA-DCM-loaded NPs indicates the concurrent encapsulation of PFV in the NPs.

Figure 2 shows the transmission electron microscopy (TEM) and field-emission scanning electron microscopy (FESEM) images of PFV/TPE-TPA-DCM co-loaded BSA NPs with [PFV RU]/[TPE-TPA-DCM] = 18.8:1. The NPs are well dispersed and spherical in shape with a nearly uniform size of ~100 nm in
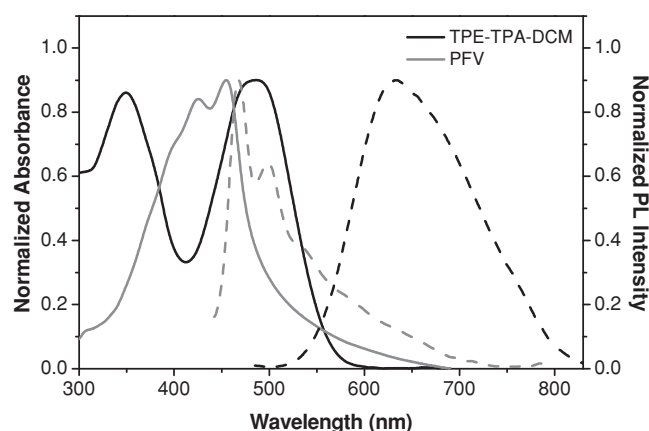

Figure 1. Normalized UV-vis absorption (solid line) and photoluminescence (PL) (dashed line) spectra of TPE-TPA-DCM (black) and PFV (gray) in THF.
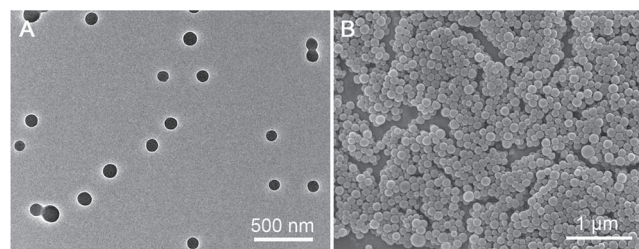

Figure 2. TEM (A) and FESEM (B) images of the PFV/TPE-TPA-DCM co-loaded BSA NPs with [PFV RU]/[TPE-TPA-DCM] = 18.8:1.
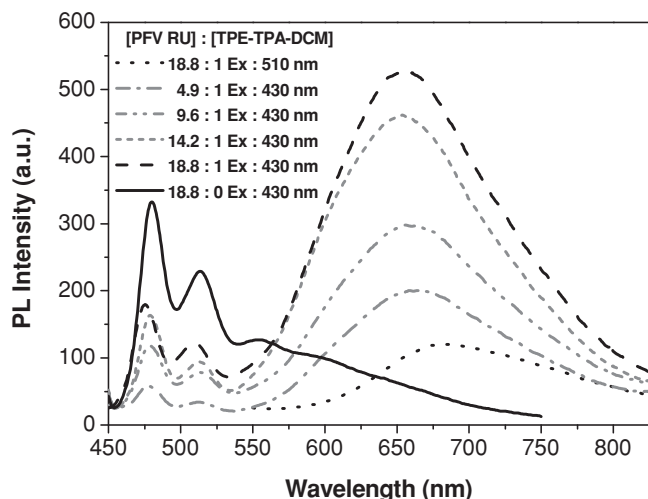
Figure 3. The PL spectra of PFV/TPE-TPA-DCM co-loaded BSA NPs in water.

both TEM and FESEM, which is smaller than the hydrodynamic diameter (159 nm) measured by LLS due to the dry sample state in TEM and FESEM observations.

The UV-vis absorption spectra of PFV-loaded, TPE-TPA-DCM-loaded, and PFV/TPE-TPA-DCM co-loaded BSA NPs in water are depicted in Figure S2 in the SI. PFV-loaded NPs share two absorption bands centered at 430 and 460 nm, respectively. These bands are red-shifted by ~5 nm, respectively, as compared to those of PFV in THF (Figure 1). TPE-TPA-DCM-loaded NPs have two absorption maxima at 358 and 510 nm, which are red-shifted by 8 and 24 nm, respectively, as compared to those of TPE-TPA-DCM in THF. As expected, PFV/TPE-TPA-DCM co-loaded BSA NPs possess the absorption peaks corresponding to PFV-loaded and TPE-TPA-DCM-loaded NPs, respectively.

Figure 3 shows the PL spectra of PFV/TPE-TPA-DCM co-loaded BSA NPs with various [PFV RU]/[TPE-TPA-DCM] from 4.9:1 to 18.8:1 (with the same TPE-TPA-DCM loading content) upon direct excitation of PFV at 430 nm. With the increasing ratio of [PFV RU]/[TPE-TPA-DCM], the acceptor emission band ranging from 550 nm to 830 nm increases at the expense of the donor emission at 480 to 512 nm. The amplification of TPE-TPA-DCM emission is evaluated by comparing the fluorescence of PFV/TPE-TPA-DCM co-loaded BSA NPs upon excitation of PFV at 430 nm with that upon direct excitation of TPE-TPA-DCM at 510 nm, which is summarized in Table S1 in the SI. The emission of TPE-TPA-DCM can be amplified up to ~5.3-fold at [PFV RU]/[TPE-TPA-DCM] = 18.8:1, demonstrating FRET between PFV and TPE-TPA-DCM in the NPs. In addition, the PFV/TPE-TPA-DCM co-loaded BSA NPs show a large Stokes shift of ~223 nm, which holds great promises for bioimaging with minimal background interference.[3]

In the following in vitro and in vivo imaging experiments, the PFV/TPE-TPA-DCM co-loaded BSA NPs with [PFV RU]/[TPE-TPA-DCM] = 18.8:1 were used because of the high fluorescence in FR/NIR region by FRET. The PFV-loaded and TPE-TPA-DCM-loaded BSA NPs with the same amount of PFV or TPE-TPA-DCM as that of PFV/TPE-TPA-DCM co-loaded NPs ([PFV RU]/[TPE-TPA-DCM] = 18.8:1) were also synthesized and used as controls. In addition, as RGD peptide can specifically target integrin receptors overexpressed in many tumor cells,[24] the PFV/TPE-TPA-DCM co-loaded BSA NPs were further modified with positively charged RGDKKKKKK peptide (isoelectric point ~ 11.2) at pH 7.4 through electrostatic interaction (Scheme 2). The content of peptide in PFV/TPE-TPA-DCM co-loaded BSA-RGD NPs with [PFV RU]/[TPE-TPA-DCM] = 18.8:1 was 6.9 μmol/g NPs measured by high performance liquid chromatography (HPLC), which corresponded to ~9700 RGD peptide immobilized on each NP. A detailed calculation is described in the SI.

2.2. Cellular Imaging

Cellular imaging based on PFV/TPE-TPA-DCM co-loaded BSA NPs with and without RGD functionalization was investigated by confocal laser scanning microscopy (CLSM). HT-29 colon cancer cells that have overexpressed integrin receptors were used as the target cells.[25] **Figures 4** A-B and 4C-D show the CLSM images of HT-29 cancer cells after incubation with PFV/TPE-TPA-DCM co-loaded BSA NPs for 2 h at 37 °C. The images were taken by collecting the signals above 650 nm upon excitation at 532 nm (0.2 mW) for Figures 4A-B and 405 nm (0.2 mW) for Figures 4C-D. As shown in Figures 4A-D, red fluorescence is observed from the cell cytoplasm, which is further verified by the corresponding 3D confocal image (Figure S3 in the SI), indicating that the PFV/TPE-TPA-DCM co-loaded BSA NPs can be internalized by the
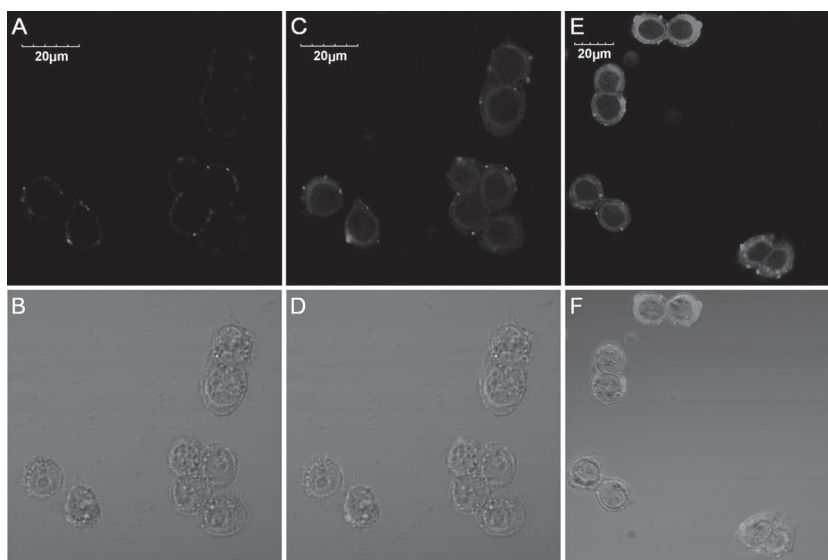

Figure 4. CLSM images of HT-29 cancer cells incubated with PFV/TPE-TPA-DCM co-loaded BSA NPs (A-D) and PFV/TPE-TPA-DCM co-loaded BSA-RGD NPs (E, F). λ_{ex} = 532 nm/λ_{em} = 650 nm for (A, B) and λ_{ex} = 405 nm/λ_{em} = 650 nm for (C-F). Fluorescence images: (A, C, E); Fluorescence/transmission overlay images: (B, D, F). Color image of Figure 4 is shown in the SI.

ADVANCED
HEALTHCARE
MATERIALS

www.advhealthmat.de

Materials
Views
www.MaterialsViews.com

cells. As the controls, HT-29 cancer cells were also incubated with PFV-loaded and TPE-TPA-DCM-loaded BSA NPs, respectively, for 2 h at 37 °C. The corresponding CLSM images were taken under the same imaging conditions for Figures 4C-D (Figure S4 in the SI). Little fluorescence signal from PFV-loaded NP-stained HT-29 cells (Figures S4A-B) and weak fluorescence from TPE-TPA-DCM-loaded NP-stained HT-29 cells (Figures S4C-D) are observed. The much higher fluorescence intensity of HT-29 cancer cells shown in Figure 4C as compared to that in Figure 4A as well as Figures S4A and S4C, demonstrates that the PFV amplified TPE-TPA-DCM fluorescence is maintained in cells.

Figures 4E-F show the CLSM images of HT-29 cancer cells after incubation with PFV/TPE-TPA-DCM co-loaded BSA-RGD NPs for 2 h at 37 °C. Under the same imaging conditions for Figures 4C-D, further enhanced fluorescence from the cellular cytoplasm (confirmed by 3D confocal image as shown in Figure S5 in the SI) is observed in Figures 4E-F. Quantitative analysis using Image Pro Plus software indicates that the average fluorescence intensity from PFV/TPE-TPA-DCM co-loaded BSA-RGD NP-stained HT-29 cells is ~2-fold higher than that from HT-29 cells in Figure 4C. These results suggest that more PFV/TPE-TPA-DCM co-loaded BSA-RGD NPs are internalized by HT-29 cancer cells due to specific binding between RGD and integrin receptors overexpressed in HT-29 cells.[25] The specific targeting ability of PFV/TPE-TPA-DCM co-loaded BSA-RGD NPs to HT-29 colon cancer cells was further assessed using MCF-7 breast cancer cells with low expression of integrin receptors in cell membrane as a control. MCF-7 cells after incubation with PFV/TPE-TPA-DCM co-loaded BSA NPs with and without RGD functionalization show no obvious difference in fluorescence intensity (Figure S6 in the SI). Moreover, quantitative studies of both PFV/TPE-TPA-DCM co-loaded BSA-RGD NP-stained cells suggest that the average fluorescence intensity from HT-29 cells in Figure 4E is ~1.9-fold higher than that from MCF-7 cells in Figure S6B. These results further verify the specific targeting ability of PFV/TPE-TPA-DCM co-loaded BSA-RGD NPs to integrin receptor-overexpressed cancer cells.

To evaluate the cytotoxicity of PFV/TPE-TPA-DCM co-loaded BSA NPs, the metabolic viability of HT-29 cancer cells after incubation with the NPs was studied at different NP concentrations. As shown in **Figure 5**, the cell viability remains >90% within 48 h
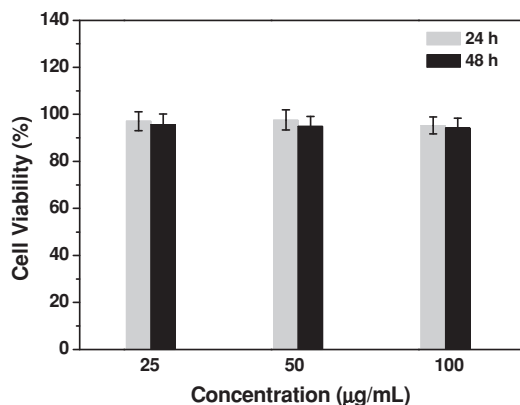

Figure 5. Metabolic viability of HT-29 colon cancer cells after incubation with PFV/TPE-TPA-DCM co-loaded BSA NP suspensions at 25, 50, and 100 μg/mL for 24 h and 48 h, respectively.
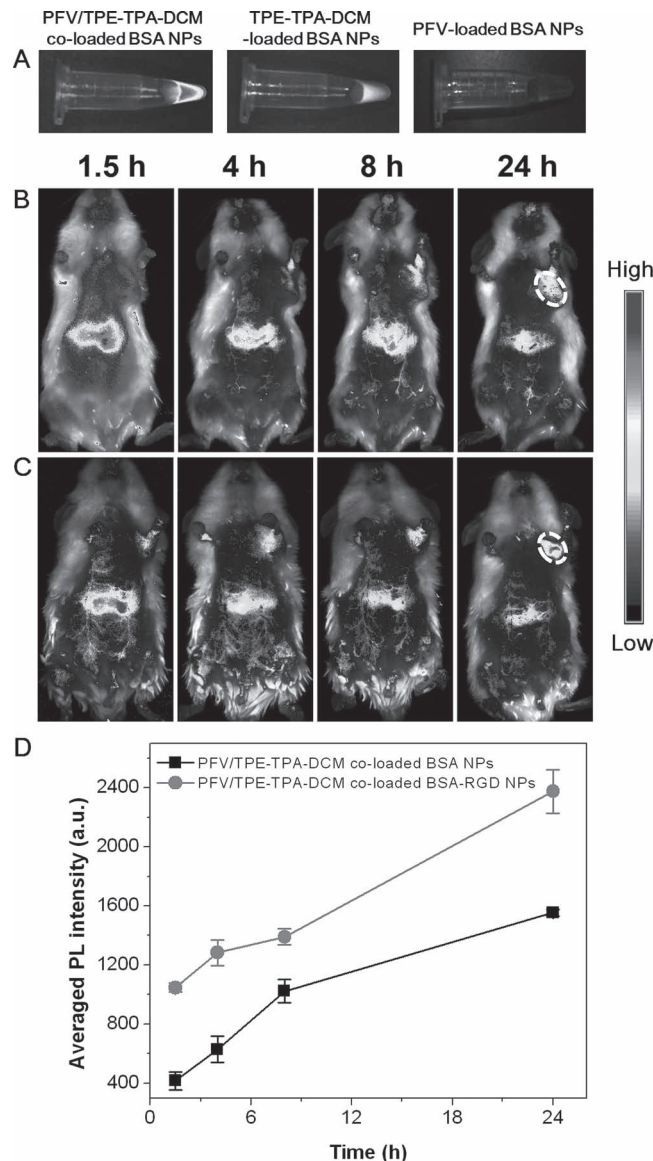

Figure 6. (A) In vitro fluorescence images of aqueous solutions containing PFV/TPE-TPA-DCM co-loaded, TPE-TPA-DCM-loaded and PFV-loaded BSA NPs. In vivo non-invasive fluorescence imaging of H$_{22}$-tumor-bearing mice after intravenous injection of PFV/TPE-TPA-DCM co-loaded BSA NPs (B), and PFV/TPE-TPA-DCM co-loaded BSA-RGD NPs (C). The white circles indicate the tumor sites. (E) Average PL intensities for the tumor tissues from the mice treated with PFV/TPE-TPA-DCM co-loaded BSA NPs and BSA-RGD NPs at various time points. Excitation at 455 nm and the signals were collected from 500–900 nm. Color image of Figure 6 is shown in the SI.

even at the highest concentration tested (100 μg/mL), suggesting low cytotoxicity of the PFV/TPE-TPA-DCM co-loaded BSA NPs.

2.3. In Vivo Live-Animal Imaging

The amplified FR/NIR signal within PFV/TPE-TPA-DCM co-loaded BSA NPs was also studied using a Maestro EX in vivo fluorescence imaging system. **Figures 6**A shows the spectral

www.MaterialsViews.com

ADVANCED
HEALTHCARE
MATERIALS
www.advhealthmat.de

FULL PAPER

imaging results obtained from PFV/TPE-TPA-DCM co-loaded NPs as well as TPE-TPA-DCM-loaded and PFV-loaded NPs in water, respectively, upon excitation at 455 nm. Using the same spectral unmixing algorithm, the acceptor fluorescence signals (from 600 to 900 nm with maximum at 660 nm, Figure S7A in the SI) were separated from the background. As shown in Figure 6A, the fluorescence intensity from PFV/TPE-TPA-DCM co-loaded NPs is much higher than that of TPE-TPA-DCM-loaded NPs and no obvious signal is observed from PFV-loaded NPs, which further indicate the signal amplification of TPE-TPA-DCM fluorescence by PFV.

In vivo FR/NIR fluorescence imaging and tumor detection based on PFV/TPE-TPA-DCM co-loaded BSA NPs with and without RGD functionalization were further studied on a tumor-bearing mouse model with the Maestro EX in vivo fluorescence imaging system. In these experiments, murine hepatic H_{22} cancer cells were subcutaneously inoculated into the left axillary space of ICR mice, affording H_{22} tumor-bearing mice. As H_{22} tumor is demonstrated to be integrin positive,[26] H_{22} tumor-bearing mice can be used to evaluate the application of PFV/TPE-TPA-DCM co-loaded BSA-RGD NPs in in vivo targeted imaging of integrin positive tumors. After intravenous injection of PFV/TPE-TPA-DCM co-loaded BSA and BSA-RGD NPs into the mice, respectively, the H_{22} tumor-bearing mice were imaged by the Maestro system at various time points. The in vivo non-invasive fluorescence images were taken upon excitation at 455 nm and the mouse autofluorescence was removed by the same spectral unmixing algorithm (Figure S7 in the SI).

Figure 6B shows the time-dependent in vivo fluorescence images of H_{22} tumor-bearing mice post intravenous injection of PFV/TPE-TPA-DCM co-loaded BSA NPs. In comparison, in vivo fluorescence image of H_{22} tumor-bearing mice at 24 h after intravenous injection of TPE-TPA-DCM-loaded BSA NPs (Figure S8 in the SI) was also taken and analyzed under the same conditions for Figure 6B. Noteworthy is that a much higher fluorescence intensity is observed from the mouse at 24 h post-injection shown in Figure 6B as compared to that in Figure S8, revealing that PFV amplified TPE-TPA-DCM signal could be used for in vivo imaging in a high contrast manner.

Moreover, as shown in Figure 6B, the fluorescence intensity in the tumor area located at the left axillary of the mouse increases over time during 24 h, indicating the accumulation of PFV/TPE-TPA-DCM co-loaded BSA NPs in tumor tissue. The elevating accumulation of NPs into tumor tissue is because of the enhanced permeability and retention (EPR) effect resulting from the tumor microenvironment such as leaky vasculature and poor lymphatic drainage, which is well known as passive tumor targeting of the NPs.[27] In comparison, the fluorescence intensity from the tumor site of mice treated with PFV/TPE-TPA-DCM co-loaded BSA-RGD NPs (Figure 6C) is higher as compared to that in Figure 6B at all tested time points. Quantitative analysis using the Maestro software indicates that the RGD functionalization of NPs endows a ~2-fold increase in fluorescence intensity of tumor tissue at all time points (Figure 6D). These results suggest that PFV/TPE-TPA-DCM co-loaded BSA-RGD NPs can achieve active tumor targeting through specific RGD-integrin recognition, making them an effective FR/NIR probe for in vivo fluorescence imaging and tumor detection in a high contrast manner. In addition, as shown in Figures 6B
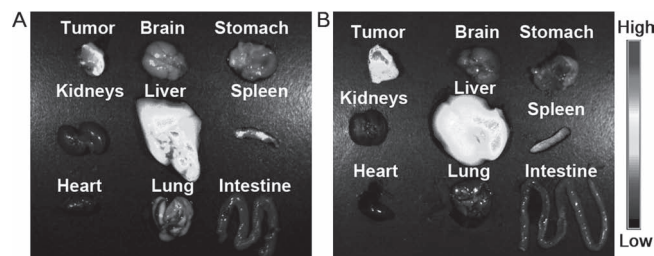

Figure 7. *Ex vivo* fluorescent imaging on tumor tissue and major organs of mice treated with PFV/TPE-TPA-DCM co-loaded BSA NPs (A) and BSA-RGD NPs (B). The mice were sacrificed at 24 h post-injection. Color image of Figure 7 is shown in the SI.

and 6C, intense fluorescence is observed in the liver area of the mice at 1.5 h post-injection because NPs generally have a tendency to undergo reticuloendothelial system (RES) organ uptake, especially the liver tissue.[28] The significant decrease in fluorescence intensity from the liver area of the mice over time suggests that the NPs can be excreted from the body through the biliary pathway from the liver to bile duct, intestine, and feces.[29] This is confirmed by the obvious fluorescence signals in the feces of mice treated with both NPs.

The mice treated with PFV/TPE-TPA-DCM co-loaded BSA NPs with and without RGD functionalization were sacrificed at 24 h post-injection and major tissues including tumor were isolated for *ex vivo* fluorescence imaging. In consistent with the results of non-invasive in vivo fluorescence imaging, the fluorescent signals are mainly observed in tumor and liver tissues and the efficient tumor targeting of RGD-functionalized NPs is also demonstrated (**Figure 7**).

3. Conclusions

In summary, we have developed a fluorescence-amplified FR/NIR probe through co-encapsulation of a CP donor (PFV) and an AIE fluorogen acceptor (TPE-TPA-DCM) into biocompatible BSA NPs. The TPE-TPA-DCM emission was amplified by up to 5.3–fold at [PFV RU]/[TPE-TPA-DCM] = 18.8:1. In addition to the high FR/NIR fluorescence, the PFV/TPE-TPA-DCM co-loaded BSA-RGD NPs showed large Stokes shift, spherical morphology and low cytotoxicity. Both in vitro and in vivo experiments revealed bright FR/NIR signals and specific targeting effect of PFV/TPE-TPA-DCM co-loaded BSA-RGD NPs for both cancer cell and live animal imaging. As probes with high FR/NIR fluorescence are of great importance for in vivo imaging and cancer diagnosis, this study provides fundamental guidelines to yield bright FR/NIR fluorescent probes using a FRET strategy and an AIE luminogen. The successful example of amplified FR/NIR emission for cellular and in vivo cancer imaging in a high contrast and selective manner will inspire more exciting research in developing novel FR/NIR fluorescent probes for improved bioimaging applications. Because of the good performance of PFV/TPE-TPA-DCM co-loaded BSA-RGD NPs in targeted in vivo imaging, we will continue to work on the detailed in vivo studies of the NPs, such as their blood circulation half-life and clearance curve of NPs via the biliary pathway.

FULL PAPER

4. Experimental Section

Materials: PFV and TPE-TPA-DCM were synthesized according to the literature.[12,21b] BSA, glutaraldehyde, trypsin-ethylenediaminetetraacetic acid (EDTA) solution, penicillin-streptomycin solution, and 3-(4,5-dimethylthiazol-2-yl)-2,5-diphenyl tetrazolium bromide (MTT) were purchased from Sigma–Aldrich (St. Louis, USA). Arginine-glycine-aspartic (RGD) acid peptide (RGDKKKKKK) was a customized product from first Base, Singapore. Fetal bovine serum (FBS) was obtained from Gibco (Lige Technologies, Switzerland). THF was distilled from sodium benzophenone ketyl under dry nitrogen immediately prior to use. Milli-Q water was supplied by a Milli-Q Plus System (Millipore Corp., Breford, USA). HT-29 colon cancer cells and MCF-7 breast cancer cells were purchased from American Type Culture Collection. Murine hepatic H_{22} cancer cells were obtained from Shanghai Institute of Cell Biology (Shanghai, China). Male ICR mice (6–8 weeks old) were provided by the animal center of Drum-Tower Hospital (Nanjing, China).

Characterization: UV-vis spectra were recorded on a Shimadzu UV-1700 spectrometer. Emission spectra were recorded on a Perkin-Elmer LS 55 spectrofluorometer. Average particle sizes of the NPs were determined by LLS with a 90 Plus particle size analyzer (Brookhaven Instruments Co., USA) at a fixed angle of 90° at room temperature. Zeta potential of the NPs was measured using a zeta potential analyzer (ZetaPlus, Brookhaven Instruments Co., USA) at room temperature. Morphology of the NPs was investigated by FESEM (JSM-6700F, JEOL, Japan) at an accelerating voltage of 10 kV. Sample was fixed on a stub with a double-sided sticky tape and then coated with a platinum layer using an autofine coater (JEOL, Tokyo, Japan) for 60 s in a vacuum at a current intensity of 10 mA. Morphology of the NPs was also studied by TEM (JEM-2010F, JEOL, Japan).

Fabrication of PFV/TPE-TPA-DCM co-Loaded BSA NPs: The PFV/TPE-TPA-DCM co-loaded BSA NPs were prepared by a modified desolvation method. Briefly, BSA (7.5 mg) was dissolved in Milli-Q water (5 mL). Subsequently, THF (8 mL, desolvation agent) containing predetermined amounts of PFV (changed from 125 to 500 µg) and TPE-TPA-DCM (fixed at 50 µg) were added dropwise into the BSA aqueous solution at room temperature under sonication using a microtip probe sonicator (XL2000, Misonix Incorporated, NY, 18 W output), which resulted in the formation of PFV/TPE-TPA-DCM co-loaded BSA NPs. Glutaraldehyde solution (50%, 5 µL) was subsequently added to cross-link the obtained NPs at room temperature for 4 h. THF was removed by rotary evaporation under vacuum. The cross-linked NP suspension was filtered through a 0.45 µm microfilter, which was then washed with Milli-Q water. The amounts of PFV/TPE-TPA-DCM loaded into the BSA NPs were determined from the absorption spectra with reference to a calibration curve of PFV and TPE-TPA-DCM in THF. The encapsulation efficiency is defined as the ratio of the amount of PFV or TPE-TPA-DCM loaded into the NPs to the total amount of PFV or TPE-TPA-DCM in the feed mixture.

Surface Functionalization: The RGD peptide functionalization of PFV/TPE-TPA-DCM co-loaded BSA NPs was performed according to the literature.[30] In brief, PFV/TPE-TPA-DCM co-loaded BSA NPs (1.5 mg) were first dispersed in 0.1 × PBS (1 mL). RGDKKKKKK solution (10^{-3} M, 20 µL) was then added into the NP suspension and gently mixed for 2 h. Subsequently, The NPs were washed three times with Milli-Q water and the supernatant was collected to determine the free RGD peptide by high performance liquid chromatography (HPLC, Shimadzu LC-ESI spectrometer). The amount of RGD peptide on each NP was determined as the ratio of the total number of immobilized peptide to the total number of NPs, which is described in detail in the SI.

Cell Culture: HT-29 colon cancer cells, MCF-7 breast cancer cells and murine hepatic H_{22} cancer cells were cultured in Dulbecco's Modified Eagle's Medium (DMEM) containing 10% fetal bovine serum and 1% penicillin streptomycin at a constant temperature of 37 °C in a humidified environment containing 5% CO_2. Prior to the imaging experiments, the cells were precultured until confluence was reached.

Cell Imaging: HT-29 cancer cells were cultured in chamber (LAB-TEK, Chambered Coverglass System, Rochester, USA) at 37 °C. After 80% confluence, the medium was removed and the adherent cells were washed twice with 1 × PBS buffer. The PFV/TPE-TPA-DCM co-loaded BSA NPs or BSA-RGD NPs with [PFV RU]/[TPE-TPA-DCM] = 18.8:1 (25 µg/mL) in FBS-free DMEM medium were then added to the chamber. After incubation for 2 h, the cells were washed three times with 1 × PBS buffer and then fixed with 75% ethanol for 20 min, which were further washed twice with 1 × PBS buffer. The stained cells were subsequently imaged by CLSM (Zeiss LSM 410, Jena, Germany) with imaging software (Olympus Fluoview FV1000). The fluorescent signals from the NPs were collected upon excitation at 405 nm (0.2 mW) or 532 nm (0.2 mW) with a 650 nm longpass barrier filter. MCF-7 cancer cells incubated with PFV/TPE-TPA-DCM co-loaded NPs with and without RGD functionalization were also studied following the same procedures.

Cytotoxicity study: Cytotoxicity of the PFV/TPE-TPA-DCM co-loaded BSA NPs against HT-29 colon cancer cells was evaluated by MTT assay. In brief, HT-29 cancer cells were seeded in 96-well plates (Costar, IL, USA) at a density of 4×10^4 cells/mL. After 24 h incubation, the cells were exposed to a series of doses of PFV/TPE-TPA-DCM co-loaded BSA NPs with [PFV RU]/[TPE-TPA-DCM] = 18.8:1 at 37 °C. To eliminate the UV absorption interference of the PFV/TPE-TPA-DCM co-loaded BSA NPs at 570 nm, the cells were incubated with the same series of doses of the NPs as the control. After the designated time intervals, the sample wells were washed twice with 1 × PBS buffer and freshly prepared MTT solution (0.5 mg/mL, 100 µL) in culture medium was added into each sample well. The MTT medium solution was carefully removed after 3 h incubation in the incubator for the sample wells, whereas the control wells without addition of MTT solution were washed twice with 1 × PBS buffer. DMSO (100 µL) was then added into each well and the plate was gently shaken for 10 min at room temperature to dissolve all the precipitates formed. The absorbance of individual wells at 570 nm was then monitored by the microplate Reader (GENios Tecan). The absorbance of MTT in the sample well was determined by the differentiation between the absorbance of the sample well and that of the corresponding control well. Cell viability was expressed by the ratio of the absorbance of MTT in the sample wells to that of the cells incubated with culture medium only.

In Vivo Fluorescence Imaging: All the animal studies were performed in compliance with the guidelines set by the Animal Care Committee at Drum-Tower Hospital. Murine hepatic H_{22} cancer cell suspension containing 5–6 × 10^6 cells (0.1 mL) were injected subcutaneously to the ICR mice (average body weight of 25 g) at the left axilla. When the tumor volume reached a mean size of about 300 mm³, the mice were intravenously injected with PFV/TPE-TPA-DCM co-loaded BSA NPs ([PFV RU]/[TPE-TPA-DCM] = 18.8:1, 1 mg/mL, 200 µL) with and without RGD functionalization, respectively. The mice were anesthetized and placed on an animal plate heated to 37 °C. The time-dependent biodistribution in mice was imaged using a Maestro EX in vivo fluorescence imaging system (CRi, Inc., Woburn, USA). The light with a central wavelength of 455 nm was selected as the excitation source. In vivo spectral imaging from 500 to 900 nm (with 10 nm step) was conducted with an exposure time of 150 ms for each image frame. The mouse autofluorescence was removed using spectral unmixing software, leaving the pure NP fluorescence. After removing the autofluorescence, the average NP fluorescence intensity in tumor tissue was calculated from the unmixed signal image using the region-of-interest (ROI) function of the Maestro software. Scans were carried out at 1.5 h, 4 h, 8 h and 24 h post-injection. In addition, the H_{22} tumor-bearing mice were also sacrificed at 24 h post intravenous injection of PFV/TPE-TPA-DCM co-loaded BSA NPs with and without RGD functionalization, respectively. The organs including brain, stomach, kidneys, liver, spleen, heart, lung, intestine and tumor were excised and imaged by the Maestro system for *ex vivo* fluorescence imaging.

Supporting Information

Supporting Information is available from the Wiley Online Library or from the author.

Materials
Views

www.MaterialsViews.com

ADVANCED
HEALTHCARE
MATERIALS
www.advhealthmat.de

FULL PAPER

Acknowledgements

[1] a) S. Kim, Y. T. Lim, E. G. Soltesz, A. M. D. Grand, J. Lee, A. Nakayama, J. A. Parker, T. Mihaljevic, R. G. Laurence, D. M. Dor, L. H. Cohn, M. G. Bawendi, J. V. Frangioni, *Nat. Biotechnol.* **2004**, *22*, 93; b) X. H. Gao, Y. Y. Cui, R. M. Levenson, L. W. K. Chung, S. M. Nie, *Nat. Biotechnol.* **2004**, *22*, 969; c) Q. Chermont, C. Chanéac, J. Seguin, F. Pellé, S. Maîtrejean, J. P. Jolivet, D. Gourier, M. Bessodes, D. Scherman, *Proc. Natl. Acad. Sci. U. S. A.* **2007**, *104*, 9266; d) K. Y. Pu, K. Li, B. Liu, *Adv. Funct. Mater.* **2010**, *20*, 2770.

[2] a) J. V. Frangioni, *Curr. Opin. Chem. Biol.* **2003**, *7*, 626; b) B. Law, C. H. Tung, *Bioconjugate. Chem.* **2009**, *20*, 1683; c) D. Ding, K. Li, Z. S. Zhu, K. Y. Pu, Y. Hu, X. Q. Jiang, B. Liu, *Nanoscale* **2011**, *3*, 1997.

[3] W. C. Wu, C. Y. Chen, Y. Q. Tian, S. H. Jang, Y. N. Hong, Y. Liu, R. R. Hu, B. Z. Tang, Y. T. Lee, C. T. Chen, W. C. Chen, A. K. Y. Jen, *Adv. Funct. Mater.* **2010**, *20*, 1413.

[4] a) J. H. Kim, Y. S. Kim, K. Park, E. Kang, S. Lee, H. Y. Nam, K. Kim, J. H. Park, D. Y. Chi, R. W. Park, I. S. Kim, K. Choi, I. C. Kwon, *Biomaterials* **2008**, *29*, 1920; b) D. Ding, J. Wang, Z. S. Zhu, R. T. Li, W. Wu, B. R. Liu, X. Q. Jiang, *ACS Appl. Mater. Interfaces* **2012**, *4*, 1838.

[5] a) B. Ballou, B. C. Lagerholm, L. A. Ernst, M. P. Bruchez, A. S. Waggoner, *Bioconjugate. Chem.* **2004**, *15*, 79; b) X. Michalet, F. F. Pinaud, L. A. Bentolila, J. M. Tsay, S. Doose, J. J. Li, G. Sundaresan, A. M. Wu, S. S. Gambhir, S. Weiss, *Science* **2005**, *307*, 538.

[6] a) U. Resch-Genger, M. Grabolle, S. Cavaliere-Jaricot, R. Nitschke, T. Nann, *Nat. Methods* **2008**, *5*, 763; b) C. F. Wu, T. Schneider, M. Zeigler, J. B. Yu, P. G. Schiro, D. R. Burnham, J. D. McNeill, D. T. Chiu, *J. Am. Chem. Soc.* **2010**, *132*, 15410.

[7] a) R. Yang, A. Garcia, D. Korystov, A. Mikhailovsky, G. C. Bazan, T. Q. Nguyen, *J. Am. Chem. Soc.* **2006**, *128*, 16532; b) S. W. Thomas, G. D. Joly, T. M. Swager, *Chem. Rev.* **2007**, *107*, 1339.

[8] C. M. Niemeyer, *Angew. Chem. Int. Ed.* **2001**, *40*, 4128.

[9] a) B. Dubertret, P. Skourides, D. J. Norris, V. Noireaux, A. H. Brivanlou, A. Alibchaber, *Science* **2002**, *298*, 1759; b) A. M. Smith, H. Duan, A. M. Mohs, S. Nie, *Adv. Drug Delivery Rev.* **2008**, *60*, 1226.

[10] a) Y. N. Hong, J. W. Y. Lam, B. Z. Tang, *Chem. Commun.* **2009**, *29*, 4332; b) Y. N. Hong, J. W. Y. Lam, B. Z. Tang, *Chem. Soc. Rev.* **2011**, *40*, 5361.

[11] Y. Yu, C. Feng, J. Z. Liu, S. J. Chen, K. M. Ng, K. Q. Luo, B. Z. Tang, *Adv. Mater.* **2011**, *23*, 3298.

[12] W. Qin, D. Ding, J. Z. Liu, W. Z. Yuan, Y. Hu, B. Liu, B. Z. Tang, *Adv. Funct. Mater.* **2012**, *22*, 771.

[13] C. F. Wu, S. J. Hansen, Q. Hou, J. B. Yu, M. Zeigler, Y. H. Jin, D. R. Burnham, J. D. McNeill, J. M. Olson, D. T. Chiu, *Angew. Chem. Int. Ed.* **2011**, *50*, 1.

[14] a) E. A. Jares-Erijman, T. M. Jovin, *Nat. Biotechnol.* **2003**, *21*, 1387; b) D. W. Brousmiche, J. M. Serin, J. M. J. Fréchet, G. S. He, T. C. Lin, S. J. Chung, P. N. Prasad, *J. Am. Chem. Soc.* **2003**, *125*, 1448; c) K. Y. Pu, Z. Fang, B. Liu, *Adv. Funct. Mater.* **2008**, *18*, 1321; d) K. Y. Pu, B. Liu, *Biosens. Bioelectron.* **2009**, *24*, 1067.

[15] a) T. Förster, In *Modern Quantum Chemistry*; O. Sinanoglou, Ed.; Academic Press: New York **1965**; b) C. Y. Chen, Y. Q. Tian, Y. J. Cheng, A. C. Young, J. W. Ka, A. K. Y. Jen, *J. Am. Chem. Soc.* **2007**, *129*, 7220.

[16] a) D. T. McQuade, A. E. Pullen, T. M. Swager, *Chem. Rev.* **2000**, *100*, 2537; b) B. Liu, G. C. Bazan, *Chem. Mater.* **2004**, *16*, 4467.

[17] a) B. Liu, G. C. Bazan, *J. Am. Chem. Soc.* **2006**, *128*, 1188; b) K. Y. Pu, B. Liu, *Adv. Funct. Mater.* **2009**, *19*, 1371.

[18] X. R. Duan, L. B. Liu, X. L. Feng, S. Wang, *Adv. Mater.* **2010**, *22*, 1602.

[19] a) A. A. Lutich, G. X. Jiang, A. S. Susha, A. L. Rogach, F. D. Stefani, J. Feldmann, *Nano Lett.* **2009**, *9*, 2636; b) Y. H. Chan, F. M. Ye, M. E. Gallina, X. J. Zhang, Y. H. Jin, I. C. Wu, D. T. Chiu, *J. Am. Chem. Soc.* **2012**, *134*, 7309.

[20] K. Y. Pu, Z. T. Luo, K. Li, J. P. Xie, B. Liu, *J. Phys. Chem. C* **2011**, *115*, 13069.

[21] a) X. L. Feng, F. T. Lv, L. B. Liu, H. W. Tang, C. F. Xing, Q. Yang, S. Wang, *ACS Appl. Mater. Interfaces* **2010**, *2*, 2429; b) K. Li, Y. T. Liu, K. Y. Pu, S. S. Feng, R. Y. Zhan, B. Liu, *Adv. Funct. Mater.* **2011**, *21*, 287; c) K. Y. Pu, B. Liu, *Adv. Funct. Mater.* **2011**, *21*, 3408.

[22] B. D. Holt, K. N. Dahl, M. F. Islam, *Small* **2011**, *7*, 2348.

[23] a) F. Q. Li, H. Su, J. Wang, J. Y. Liu, Q. G. Zhu, Y. B. Fei, Y. H. Pan, J. H. Hu, *Int. J. Pharm.* **2008**, *349*, 274; b) S. Wagner, F. Rothweiler, M. G. Anhorn, D. Sauer, I. Riemann, E. C. Weiss, A. Katsen-Globa, M. Michaelis, J. Cinatl Jr., D. Schwartz, J. Kreuter, H. von Briesen, K. Langer, *Biomaterials* **2010**, *31*, 2388.

[24] a) E. Ruoslahti, *Annu. Rev. Cell Dev. Biol.* **1996**, *12*, 697; b) N. Nasongkla, X. Shuai, H. Ai, B. D. Weinberg, J. Pink, D. A. Boothman, *Angew. Chem. Int. Ed.* **2004**, *43*, 6323; c) K. Y. Pu, K. Li, B. Liu, *Chem. Mater.* **2010**, *22*, 6736.

[25] A. Wadih, R. Pasqualini, E. Ruoslahti, *Science* **1998**, *279*, 377.

[26] a) P. F. Liu, H. Z. Wang, Y. G. Li, Y. R. Duan, *J. Macromol. Sci. A* **2009**, *46*, 1024; b) Z. C. Liu, J. Wang, P. Yin, J. H. Qiu, R. Z. Liu, W. Z. Li, X. Fan, X. F. Cheng, C. X. Chen, J. K. Zhang, G. H. Zhuang, *Cell. Mol. Immunol.* **2009**, *6*, 285; c) Y. H. Wu, X. J. Qiao, S. Y. Qiao, L. Yu, *Expert Opin. Ther. Targets* **2011**, *15*, 421.

[27] a) L. E. van Vlerken, Z. F. Duan, S. R. Little, M. V. Seiden, M. M. Amiji, *Mol. Pharmaceut.* **2008**, *5*, 516; b) O. C. Farokhzad, R. Langer, *ACS Nano* **2009**, *3*, 16.

[28] a) S. D. Li, L. Huang, *Mol. Pharmaceut.* **2008**, *5*, 496; b) D. Ding, Z. S. Zhu, R. T. Li, X. L. Li, W. Wu, X. Q. Jiang, B. R. Liu, *ACS Nano* **2011**, *5*, 2520.

[29] Z. Liu, C. Davis, W. Cai, L. He, X. Y. Chen, H. J. Dai, *Proc. Natl. Acad. Sci. U. S. A.* **2008**, *105*, 1410.

[30] K. Li, R. Y. Zhan, S. S. Feng, B. Liu, *Anal. Chem.* **2011**, *83*, 2125.